Discovery of BBO-8520, a first-in-class direct and covalent dual inhibitor of GTP-bound (ON) and GDP-bound (OFF) KRAS^{G12C}

Anna E. Maciag[1]*, James P. Stice[2]*, Bin Wang[2]*, Alok K. Sharma[1], Albert H. Chan[1], Ken Lin[2], Devansh Singh[2], Marcin Dyba[1], Yue Yang[3], Saman Setoodeh[2], Brian P. Smith[1], Jin Hyun Ju[2], Stevan Jeknic[2], Dana Rabara[1], Zuhui Zhang[2], Erik K. Larsen[1], Dominic Esposito[1], John-Paul Denson[1], Michela Ranieri[4], Mary Meynardie[4], Sadaf Mehdizadeh[2], Patrick A. Alexander[1], Maria Abreu Blanco[1] , David M. Turner[1], Rui Xu[2], Felice C. Lightstone[3], Kwok-Kin Wong[4], Andrew G. Stephen[1], Keshi Wang[2], Dhirendra K. Simanshu[1], Kerstin W. Sinkevicius[2], Dwight V. Nissley[1], Eli Wallace[2], Frank McCormick[1,5] #, Pedro J. Beltran[2] #

[1]NCI RAS Initiative, Cancer Research Technology Program, Frederick National Laboratory for Cancer Research, Leidos Biomedical Research, Inc., Frederick, Maryland 21701, USA

[2] BridgeBio Oncology Therapeutics, 1 Corporate Drive, South San Francisco, California 94080 USA

[3] Physical and Life Sciences (PLS) Directorate, Lawrence Livermore National Laboratory, Livermore, California 94550, USA

[4] Perlmutter Cancer Center, New York University, New York, NY, USA

[5] Helen Diller Family Comprehensive Cancer Center, University of California San Francisco, 1450 3rd Street, San Francisco, California 94158, USA

* These authors contributed equally

Please address correspondence to:

Pedro Beltran, PhD

Pedro.beltran@bridgebiooncology.com

BridgeBio Oncology Therapeutics

1 Corporate Drive

South San Francisco, CA 94080

Ph: 805-217-3274

Frank McCormick, PhD, FRS

Frank.mccormick@ucsf.edu

UCSF Helen Diller Family Comprehensive Cancer Center,

Room HD-371

1450 3rd Street,

San Francisco, CA 94158-9001

Ph: 415 218 0155

Keywords: GTPase KRAS, KRAS G12C, BBO-8520, Small Molecule Inhibitor, Cancer

Running Title: BBO-8520 a first-in-class dual $KRAS^{G12C}$ Inhibitor for NSCLC

Disclosure of Potential Conflicts of Interest

All BridgeBio Oncology Therapeutics (BBOT) authors are employees and stockholders of BBOT, a private company. This research received no external funding.

Abstract

Approved inhibitors of $KRAS^{G12C}$ prevent oncogenic activation by sequestering the inactive, GDP-bound (OFF) form rather than directly binding and inhibiting the active, GTP-bound (ON) form. This approach provides no direct target coverage of the active protein. Expectedly, adaptive resistance to $KRAS^{G12C}$ (OFF)-only inhibitors is observed in association with increased expression and activity of $KRAS^{G12C}$(ON). To provide optimal $KRAS^{G12C}$ target coverage, we have developed BBO-8520, a first-in-class, direct dual inhibitor of $KRAS^{G12C}$(ON) and (OFF) forms. BBO-8520 binds in the Switch-II/Helix3 pocket, covalently modifies the target cysteine and disables effector binding to $KRAS^{G12C}$(ON). BBO-8520 exhibits potent signaling inhibition in growth factor activated states where current (OFF)-only inhibitors demonstrate little measurable activity. *In vivo*, BBO-8520 demonstrates rapid target engagement and inhibition of signaling, resulting in durable tumor regression in multiple models, including those resistant to $KRAS^{G12C}$(OFF)-only inhibitors. BBO-8520 is in Phase 1 clinical trials in patients with $KRAS^{G12C}$ non-small cell lung cancer (NSCLC).

Statement of Significance

BBO-8520 is a first-in-class direct, small molecule covalent dual inhibitor that engages $KRAS^{G12C}$ in both the active (ON) and inactive (OFF) conformations. BBO-8520 represents a novel mechanism of action that allows for optimal target coverage and delays the emergence of adaptive resistance seen with (OFF)-only inhibitors in the clinic.

Introduction

RAS is the most frequently mutated oncogene in human cancer. *RAS* mutations occur in approximately 260,000 new cancer cases per year in the United States, and 3.4 million per year worldwide [1]. *RAS* genes encode small GTPase proteins which cycle between active GTP-bound (ON) and inactive GDP-bound (OFF) states. In the (ON) state, RAS activates multiple downstream signaling pathways, including the mitogen-activated protein kinase (MAPK) and phosphoinositide 3-kinase (PI3K) pathway, promoting proliferation, migration, and survival [2]. $KRAS^{G12C}$ is an oncogenic mutation which leads to insensitivity to GTPase activating protein (GAP)-mediated hydrolysis, which significantly increases the proportion of $KRAS^{G12C}$ in the (ON) state and promotes tumor cell growth [2]. $KRAS^{G12C}$ mutations are found in approximately 14% of non-small cell lung cancers (NSCLCs), 3% of colorectal cancers (CRCs), and 1% of pancreatic cancers [3].

Sotorasib (AMG-510, LUMAKRAS™) and adagrasib (MRTX-849, KRAZATI™) are allele-specific $KRAS^{G12C}$(OFF) covalent inhibitors, which have been approved for patients with $KRAS^{G12C}$ locally advanced or metastatic NSCLC [4-6]. While these inhibitors have improved the treatment paradigm for patients with tumors harboring $KRAS^{G12C}$ mutations, they are limited with regards to the depth and duration of response, which are suboptimal compared to other driver-targeted therapies in NSCLC, like osimertinib and alectinib [7, 8]. This suboptimal efficacy from (OFF)-only inhibitors is likely driven by cancer cell adaptation through increasing the amount of drug-insensitive $KRAS^{G12C}$(ON) [9-11]. Patient responses may be improved with a compound that can inhibit $KRAS^{G12C}$(ON). In fact, clinical data from RMC-6291 [12], a $KRAS^{G12C}$(ON)-only inhibitor that depends on a

tri-complex formation with cyclophilin A, has recently reported an objective response rate of 50% in NSCLC patients with recent prior $KRAS^{G12C}$(OFF)-only inhibitor treatment [13].

Here we introduce BBO-8520, a potent, selective, orally bioavailable, direct covalent inhibitor of $KRAS^{G12C}$, with dual activity against both the (OFF) and (ON) states of $KRAS^{G12C}$. BBO-8520 is predicted to be more efficacious than sotorasib and adagrasib due to optimal target coverage of both the (ON) and (OFF) states, increased target engagement, and the potential to overcome sotorasib and adagrasib resistance mechanisms, including $KRAS^{G12C}$ amplification and activation of receptor tyrosine kinases (RTKs).

Results

Identification of BBO-8520

While exploring the druggable space in the Switch-II/Helix3 pocket of KRAS, we identified compound **1,** with a quinazoline scaffold, which displayed a dissociation constant (K_D) of 0.009 μM with GDP-bound $KRAS^{G12D}$ and sub-micromolar affinity (K_D of 0.52 μM) binding to $KRAS^{G12D}$ in the active conformation bound to nonhydrolyzable GTP analogue GppNHp **(Fig. 1A)**. We hypothesized that binding of compound **1** to $KRAS^{G12D}$(ON) may cause conformational changes in the protein leading to disruption of RAS/effector interaction. To evaluate the effectiveness of compound **1** in disrupting $KRAS^{G12D}$ and RAF1 binding, we used a biochemical protein-protein interaction (PPI) HTRF (Homogeneous Time-Resolved Fluorescence) assay. Compound **1** disrupted $KRAS^{G12D}$ binding to the RAS-binding domain (RBD) of RAF1 with an IC_{50} of 1.4 μM.

This measurable noncovalent activity against $KRAS^{G12D}$(ON) inspired the development of dual inhibitors that could bind covalently to cysteine 12 in both (ON) and (OFF) states of $KRAS^{G12C}$. Adding an acrylamide warhead to compound **1** gave rise to compound **2**. Using a MALDI-TOF mass spectrometry-based assay, we evaluated target engagement in $KRAS^{G12C}$ proteins in both (ON) and (OFF) conformations. Compound **2** showed covalent modification of C12 in the (ON) state of $KRAS^{G12C}$ although to a lesser degree than in the (OFF) state **(Fig. 1B)**. Interestingly, the ability to modify $KRAS^{G12C}$ (ON) translated to strong activity in the $KRAS^{G12C}$/RAF1(RBD) PPI disruption assay with an IC_{50} of 140 nM (**Fig. 1B)**. Further modification of the quinazoline 2- and 4-positions to improve cell potency and ADME properties (clearance and oral bioavailability) gave rise to compound **3**. Although compound **3** showed equal potency against the GDP- and GppNHp-bound proteins in the MALDI-TOF assay (>90% modification), it lost significant potency when the natural ligand (GTP) was used instead of the non-hydrolysable analogue GppNHp (38% modified). The loss of potency against the GTP-bound protein was also observed in the PPI assay where the 120 nM IC_{50} for GppNHp-bound protein shifted 30-fold with the GTP-bound protein **(Fig. 1B).** This discrepancy could be attributed to an artificial increase in State 1 conformation of $KRAS^{G12C}$ protein resulting from the use of the nucleotide mimetic [14].

Further optimization using structure-based drug design to improve binding to $KRAS^{G12C}$ identified BBO-8520 (**Fig. 1A**), a potent, selective, and direct dual inhibitor of $KRAS^{G12C}$ in both (ON) and (OFF) states. BBO-8520 engaged the target cysteine (C12) rapidly, regardless of nucleotide status, including GTP, as evidenced by MALDI-TOF mass spectrometry measurements (**Fig. 1B**). BBO-8520 also potently disrupted

KRAS^{G12C}/RAF1(RBD) interaction with an IC_{50} of less than 100 nM whether KRAS^{G12C} was bound to GppNHp or GTP (**Fig. 1B**). As expected, both sotorasib and adagrasib showed no activity in this assay.

To confirm the improved potency of BBO-8520 in comparison to sotorasib and adagrasib, we determined the K_{inact}/K_I of sotorasib, adagrasib, and BBO-8520 using a mass spectrometry-based method as well as measuring the inhibition of pERK in NCI-H358 cells. BBO-8520 had a K_{inact}/K_i of 20,000 $M^{-1}s^{-1}$ in GTP-bound (ON) and 2,743,000 $M^{-1}s^{-1}$ in GDP-bound (OFF) KRAS^{G12C}, compared to sotorasib and adagrasib which had no activity against (ON), and 11,000 and 180,000 $M^{-1}s^{-1}$ against (OFF) conformations of the protein, respectively (**Fig. 1C and Supplementary Fig. S1A-D**). In the heterozygous KRAS^{G12C} cell line, NCI-H358, BBO-8520 had a K_{inact}/K_i of 43,000 $M^{-1}s^{-1}$ compared to 1,064 $M^{-1}s^{-1}$ for adagrasib and 776 $M^{-1}s^{-1}$ for sotorasib for a 40 and 55-fold increase, respectively **(Supplementary Fig. S1E&Fs).** BBO-8520 consistently showed stronger activity against the KRAS^{G12C}(OFF) protein than the KRAS^{G12C} (ON) state in all assays.

BBO-8520 binds to both (ON) and (OFF) KRAS^{G12C} as revealed by crystal structures

To gain structural insights into the binding modes of BBO-8520 to KRAS^{G12C}, we tethered the compound to GDP- and GppNHp-bound proteins and solved their crystal structures at 1.67 Å and 2.10 Å resolution, respectively **(Supplementary Table S1)**. Both crystal structures showed a high degree of similarity, with BBO-8520 binding in the pocket between Switch-II and alpha Helix 3 **(Fig. 2A)**. The Switch-I region responsible for binding effectors adopts the open conformation in both structures. While Switch-I does not interact with BBO-8520 directly, its C-terminal end is affected by the conformation that

158 Switch-II adopts to accommodate the ligand. Importantly, in the GppNHp-bound structure,
159 Switch-I moves away from the nucleotide, adopting a state 1 conformation that is not
160 compatible with effector-binding. This conformation, also detected by ^{31}P NMR as
161 described below, is characterized by the loss of direct coordination between the hydroxyl
162 group of T35 and the Mg^{2+} ion.

163 In the interaction of BBO-8520 with $KRAS^{G12C}$(OFF), the quinazoline core is
164 sandwiched between E62 and Y96, and the nitrogen at the N1 position makes a H-bond
165 with the H95 side chain **(Fig. 2B)**. At the C2 position, the pyrrolizidine group rests between
166 H95 and D92, and its positively charged nitrogen makes a salt bridge with E62. The CF_3
167 at the C6 position and the aminobenzothiophene at the C7 position make extensive van
168 der Waals contacts with residues in the C-terminal halves of Switch-II and Helix 3.
169 Furthermore, the amino group of the aminobenzothiophene forms H-bonds with the D69
170 side chain and the backbone carbonyl of E63. The cyano group substituted at the 3-
171 position of the aminobenzothiophene makes a H-bond with the backbone NH of E63.
172 Alternatively, it could engage in a water-mediated interaction with R68. At the C4 position,
173 the dimethylpiperazine adopts a chair conformation with the 2-methyl pointing towards
174 A59 of Switch-II and the 5-methyl sandwiched between the C12 sulfur and the quinazoline
175 N3 nitrogen **(Fig. 2C)**. The acrylamide vinyl forms a covalent bond with the sulfur of C12,
176 and the acrylamide carbonyl makes a H-bond with the K16 side chain.

177 In the (ON) structure, the interactions between BBO-8520 and $KRAS^{G12C}$ remained
178 largely the same, with the quinazoline core, pyrrolizidine, CF_3 and aminobenzothiophene
179 making the same H-bond and salt bridge contacts with E62, E63, R68, D69 and H95 **(Fig.**
180 **2D)**. However, at the C4 position, the dimethylpiperazine rotates by ca. 180°, such that

the 5-methyl points towards Switch-II and makes van der Waals contacts with both A59 and G60, while the 2-methyl sits next to the quinazoline N3 nitrogen **(Fig. 2E)**. This rotation is triggered by the repositioning of the acrylamide, necessary because the carbonyl is now too close (2 Å) to the gamma-phosphate of the GppNHp **(Fig. 2F-G)**. Consequently, this rotation results in the loss of the H-bond between the acrylamide carbonyl and the K16 side chain that is partially compensated by the van der Waals contact with the G60 backbone **(Fig. 2E)**. Overall, the BBO-8520 binding pose is very similar in both structures, especially for the aminobenzothiophene component, while the slight tilt of the core is well accommodated by the protein **(Fig. 2F)**. These properties allow BBO-8520 to bind tightly to both (ON) and (OFF) states of $KRAS^{G12C}$, although its affinity for $KRAS^{G12C}$(ON) is lower likely due to the loss of the H-bond to K16. The electron density maps of BBO-8520 bound to $KRAS^{G12C}$ in both (ON) and (OFF) states are shown in **Supplementary Fig. S2A-D**.

BBO-8520 displays a dual (ON/OFF) mechanism of action and differential selectivity for $KRAS^{G12C}$

In solution, GTP-bound (ON) RAS exists in two interconverting conformational states, state 1 (signaling incompetent) and state 2 (signaling competent). This can be observed as two separate γ phosphate (γP) peaks (γ_1 and γ_2, respectively) in ^{31}P NMR spectroscopy. When in complex with effector RAF1(RBD), the state 2 conformation of RAS is stabilized.

We investigated perturbation of the $KRAS^{G12C}$(ON) state 1 - state 2 conformational equilibrium upon BBO-8520 binding using ^{31}P NMR. As depicted in **Fig. 3A**, BBO-8520

binding significantly alters the protein conformational equilibrium resulting in the emergence of a new predominant γ_1Protein-Ligand (γ_{1PL}) peak at ~ -4.5 ppm, and a reduced γ_1 peak (< 10% of peak intensity relative to γ_{1PL}). The γ_{1PL} peak represents a "state 1 – like" (signaling incompetent) inactive conformation. This perturbation profile strongly resembles that reported recently for KRAS^{G12C}(ON) binding of a close analog of BBO-8520 [14]. A considerable perturbation is also noted for the β peak (shifted by -1.4 ppm relative to β_2), however, to a lesser degree than noted for the γ peak, whereas the α peak is mostly unaffected. Importantly, the signaling competent conformer (γ_2) is not apparent in the spectrum. The downfield shift of γ_{1PL} from γ_1 in the protein-ligand (PL) complex is largely due to the induced displacement of the Switch-I region away from the nucleotide and suggests that the strong inhibitory effect of BBO-8520 is due to forcing KRAS^{G12C} into a signaling incompetent (inactive) conformation.

The addition of equimolar RAF1(RBD) to KRAS^{G12C}(ON) in the PL binary sample induces a conformational redistribution by shifting nearly half of the γ_{1PL} peak to γ_1 only, representing effector binding-deficient state 1, and does not shift back to the signaling-competent state 2 **(Fig. 3A)**. Spoerner *et al* noted that RAS mutants were non-oncogenic if the presence of effector protein was unable to shift the state 1 conformation to state 2 [15]. The inability of RAF1(RBD) to induce state 2 in the KRAS^{G12C}(ON) – BBO-8520 complex indicates that the compound forces the GTP-bound (ON) protein into the inactive, effector binding-deficient conformation. This NMR-based mechanistic data, together with evidence provided on **Fig. 3B** that BBO-8520 potently inhibits SOS-mediated nucleotide exchange, demonstrate a dual mechanism of action encompassing

inducing the state 1 (effector binding deficient) conformation in $KRAS^{G12C}$ (ON) as well as locking $KRAS^{G12C}$(OFF) in its inactive state.

Next, we used mouse embryonic fibroblasts (MEFs) expressing unique RAS isoforms, and KRAS mutants, to test the potency and selectivity of BBO-8520 [16]. Treatment of MEFs with BBO-8520 showed no activity against HRAS, NRAS and $BRAF^{V600E}$ (IC_{50}>10 mM) confirming exquisite selectivity for the KRAS protein. As expected, BBO-8520 displayed the highest activity against $KRAS^{G12C}$ with single digit nM IC_{50} on pERK inhibition (>10x better than sotorasib and adagrasib) **(Fig.3C)**. Interestingly, the improved noncovalent interactions within the binding pocket allowed BBO-8520 to gain potency against other KRAS mutant isoforms or WT protein. This was also observed in the nucleotide exchange data on **Fig 3B**. BBO-8520 showed potency against $KRAS^{G13D}$ and WT KRAS4b (albeit at 5-10x lower than $KRAS^{G12C}$). Activity against other KRAS mutant isoforms was measurable but right shifted >100-fold from $KRAS^{G12C}$ activity and may not be biologically significant in the *in vivo* or clinical settings.

BBO-8520-induced conformational changes within Switch I/II region translate to a rapid and potent inhibition of oncogenic signaling

BBO-8520 showed rapid (within 30 min) engagement of Cys-12 in the $KRAS^{G12C}$ mutant MIA PaCa-2 and SW1463 cell lines, leading to $KRAS^{G12C}$ covalent modification and strong pERK signal suppression, consistent with its dual (ON/OFF) mechanism of action **(Fig. 4A)**. This early effect, only achievable by engaging $KRAS^{G12C}$ (ON), was absent from sotorasib and adagrasib even at 5x higher concentrations (100 nM) **(Fig. 4A)**. Peak downregulation of MAPK signaling pathway was observed within the first 2

hours (hrs) and lasted for at least 24 hrs in both cell lines. A time course of pERK inhibition using HTRF, as a complementary method, in both MIA PaCa-2 and SW1463 cells confirmed the rapid and sustained inhibition of ERK phosphorylation by BBO-8520 **(Fig. 4B).**

To better understand potency and selectivity of BBO-8520 in malignant cells, we then profiled the compound in a panel of ~50 cancer cell lines harboring either wild type or mutant KRAS (G12C, G12D, G12S, G12V and G13D), or a $BRAF^{V600E}$ mutation. Cells were assayed for pERK after treatment with compounds for 2 hrs, pAKT after treatment for 4 hours, or in a 7-day spheroid 3-dimensional (3D) viability assay **(Fig. 4C, D, E)**. BBO-8520 compared favorably against sotorasib and adagrasib in both the ERK phosphorylation inhibition, and 3D viability assays displaying better than 10-fold gain in potency **(Supplementary Table 2)**. Comparison with RMC-6291 in six $KRAS^{G12C}$ cell lines showed similar potency for both compounds. BBO-8520 demonstrated selectivity for $KRAS^{G12C}$ over other KRAS codon 12 mutations (50- to 500- fold selectivity for pERK and 500- to 30,000-fold for 3D viability), G13D mutations (18-fold for pERK and 390-fold for 3D viability), wild type KRAS (>1600-fold for pERK and >450-fold for 3D viability) and had no demonstrable activity in the $BRAF^{V600E}$ mutant cell line A375 (>10,000 nM IC_{50} for pERK and 3D viability) **(Fig. 4C, E)**. BBO-8520 also demonstrated potent inhibition of pAKT signaling in some $KRAS^{G12C}$ cell lines with IC_{50} below 10 nM **(Fig. 4D).**

BBO-8520 is potent against GTP-bound $KRAS^{G12C}$ in malignant cells

Evidence supporting the engagement of BBO-8520 with $KRAS^{G12C}$(ON) in malignant cells was first acquired using a RAS:RAF ELISA assay. This assay measures

KRAS^{G12C}(ON) by capturing it with the RAS-binding domain of RAF1. As shown in **Fig. 5A**, BBO-8520 started to inhibit the RAF1(RBD):KRAS^{G12C}(ON) interaction within the first 2 minutes (mins) of treatment. In striking contrast to (OFF)-only inhibitors, BBO-8520 achieved complete inhibition of KRAS^{G12C}(ON) within 15 mins. At this early time point, (OFF)-only inhibitors, sotorasib, adagrasib, and GDC-6036 only reached 20% inhibition while requiring more than 60 mins to achieve maximal activity. Further analysis of the KRAS^{G12C}(ON) inhibitory activity of BBO-8520 was performed by artificially increasing the amount of cellular GTP-bound KRAS^{G12C} through growth factor stimulation. We serum-starved NCI-H358 cells and stimulated them either with epidermal growth factor (EGF) in the presence or absence of (OFF)-only inhibitors or BBO-8520. Measurement of pERK inhibition showed that BBO-8520 retained potency in the presence of EGF while (OFF)-only inhibitors displayed a large loss of potency **(Fig. 5B)**. In a parallel experiment, NCI-H358 cells were stimulated with hepatocyte growth factor (HGF) in the presence or absence of compounds for a viability endpoint. As observed in the EGF stimulation experiment, (OFF)-only inhibitors lost potency to a much greater extent than BBO-8520 in the presence of HGF **(Fig. 5C)**. Final validation of BBO-8520's activity against the (ON) state was gathered using a HeLa cell inducible model, in which doxycycline treatment was used to express a KRAS$^{G12C/A59G}$ double mutant. A59G is a transition state mutant that abrogates GTPase activity and locks KRAS in the (ON) conformation [4]. In this system, the inhibitory effect of sotorasib or adagrasib on MAPK signaling was significantly attenuated. In contrast, BBO-8520 retained potent activity (**Fig. 5D**).

We hypothesized that the dual activity of BBO-8520 would be beneficial to address development of resistance. First, we tested the activity of BBO-8520 on previously

described acquired resistance mutations. We generated Ba/F3 cells with a series of $KRAS^{G12C}$ mutations that have altered states of GTP hydrolysis [9, 10]. As demonstrated in **Fig. S3A&B**, BBO-8520 demonstrated activity on all mutants tested in the Ba/F3 cell system. Secondly, we analyzed whether BBO-8520's dual activity could delay the onset of resistance. Using concentrations equivalent to the IC_{90} of each compound by a 2 hr pERK HTRF assay, we treated NCI-H358 cells in a 2D viability clonogenic assay and observed that BBO-8520 caused complete growth suppression up to 35 days in culture, as compared to (OFF)-only inhibitors that allowed resistance to emerge between days 18-20 (**Fig. 5E**). This demonstrates that the dual activity of BBO-8520 could drive deeper tumor responses and delay the development of resistance.

Cysteine-proteome profiling and transcriptional regulation changes confirm selectivity for $KRAS^{G12C}$

A risk associated with the use of covalent inhibitors is the potential for non-specific, off-target reactivity with cysteine residues in the proteome. To determine the selectivity of the BBO-8520 covalent interaction with $KRAS^{G12C}$, and to identify potential off-target liabilities, cysteine-proteome profiling by mass spectrometry was performed as previously described [17]. After 2 hr treatment with DMSO or 20 nM BBO-8520, the cysteine proteome was enriched, and peptides were identified. The Cys12 peptide from $KRAS^{G12C}$ was the most significantly engaged cysteine (p-value=7.1e-5, 98.9% decrease) in the analyzed proteome **(Fig. S4A).** DUS4 (p=3.3e-4, 62.9% decrease) also demonstrated reduction at two separate cysteines upon BBO-8520 treatment, suggesting downregulation of the protein rather than selective binding with BBO-8520.

Head-to-head RNA-seq studies with sotorasib (1 μM) and adagrasib (300 nM) were performed to compare the global transcriptional regulation driven by BBO-8520 in MIA PaCa-2 cells. Analysis revealed the strongest repression of genes involved in DNA replication and cell cycle progression **(Fig. S4B)**. A comparison with the gene set identified using adagrasib in NCI-H1373 and NCI-H358 cells [6] showed similar strong repression of MAPK signaling (DUSP4/6, ETV4/5, SPRY2/4) but at a 10-fold lower concentration of BBO-8520 (30 nM compared to 300 nM of adagrasib). Gene set enrichment analysis (GSEA) of the 50 hallmark signatures was performed on the differentially regulated genes from the MIA PaCa-2 RNA-seq study. A heatmap of the GSEA demonstrates a significant overlap in the signatures with all 3 compounds strongly supporting a common mechanism of action **(Fig. S4C)**. To determine if any kinases were hit by BBO-8520 leading to potential off-target effects, we performed a kinomescan on 468 kinases **(Fig. S4D).** We found that 1 μM BBO-8520 had binding activity on only 3 kinases (93% inhibition of CDK8, 87% inhibition of CDK11, and 86% inhibition of HIPK1). Follow-up biochemical dose response data for these 3 kinases showed Kd (nM) of 150, 4,600 and 10,000 for CDK11, CDK8 and HIPK1, respectively. These studies demonstrate that BBO-8520 is selective for $KRAS^{G12C}$, induces global transcriptional regulation changes highly similar to other $KRAS^{G12C}$ inhibitors, and carries low likelihood of off-target activity.

BBO-8520 exhibits robust *in vivo* efficacy

The *in vivo* potency of BBO-8520 was first measured in a single dose PK/PD Matrigel plug assay using MIA PaCa-2 cells. Following an oral dose of 3, 10, or 30 mg/kg

of BBO-8520, a statistically significant reduction in pERK was observed in all groups with 46%, 73%, and 92% pERK inhibition, respectively (**Fig. 6A**). The pERK IC_{50} was 85 nM. Similar potency was observed using MIA PaCa-2 tumors, with a pERK IC_{50} of 61 nM **(Fig. S5A**). The *in vivo* EC_{50} was consistent with the free fraction adjusted *in vitro* IC_{50} of 55 nM. Evaluation of time-dependent pERK inhibition at 2, 6, 24, 48, and 72 hrs following a single dose of BBO-8520 (30 mg/kg) resulted in 40%, 92%, 83%, 57%, and 41% pERK inhibition, respectively **(Fig. 6B)**. In the MIA PaCa-2 PK/PD tumor model, pERK inhibition correlated well (R^2=0.84) with tumor target engagement as assessed by a band shift assay on $KRAS^{G12C}$ by western blot analysis **(Fig. S5A, B)**.

The efficacy of BBO-8520 was first assessed in the MIA PaCa-2 CDX tumor model. Following daily oral dosing of BBO-8520 for 28 days at 0.1, 0.3, 1, 3, or 10 mg/kg, we observed statistically significant tumor growth inhibition of 21%, 49%, 69%, 99%, and 90% mean tumor volume regression, respectively **(Fig. 6C)**. The ED_{50} was 0.3 mg/kg and ED_{90} was 1.8 mg/kg. All treatments were well tolerated **(Supplementary Fig. S5C)**. Efficacy was also studied in the NSCLC, heterozygous $KRAS^{G12C}$ model, NCI-H358. Orally administered BBO-8520, once daily for 28 days at 0.3, 1, 3, or 10 mg/kg resulted in tumor volume reductions of 20% and 71%, and mean tumor regressions of 19% and 100%, respectively. The ED_{50} was 0.6 mg/kg and ED_{90} was 1.6 mg/kg **(Fig. 6D)**. Tumors from 1/10 and 10/10 mice in the 3 mg/kg and 10 mg/kg BBO-8520 groups, respectively, had complete regressions (CRs).

The efficacy of BBO-8520 was also tested in two syngeneic, orthotopic and immunocompetent models to assess the role of the organ microenvironment and the immune system. Our first model was the $KRAS^{G12C}$; $Tp53^{R270H}$ (KCP) NSCLC genetically

engineered mouse model (GEMM) [18]. Lung-tumor bearing KCP mice were orally administered vehicle or 10 mg/kg BBO-8520 once daily for 42 days. Statistically significant anti-tumor activity was observed following daily oral treatments with BBO-8520, with 56% mean tumor regression and no signs of resistance developing over the course of the study **(Fig. 6E)**. These results were similar to those reported with the combination of a $KRAS^{G12C}$ (OFF) inhibitor and SHP2 inhibitor in this model [19]. Our second model was a CT-26-$KRAS^{G12C}$ liver tumor model. Liver tumor-bearing mice were orally administered vehicle or 10 mg/kg BBO-8520 once daily until day 28, 10 mg/kg anti-PD-1 intraperitoneally twice weekly until day 21, or the combination of BBO-8520 and anti-PD-1. Notably, 40% (4/10) of the mice treated with BBO-8520 survived until the end of the study and were confirmed to have complete tumor regressions by IVIS imaging and necropsy. The combination of BBO-8520 and anti-PD-1 was also highly efficacious, with 60% (6/10) of the mice survived confirmed cured. The median survival was 34 days in the vehicle group. The median survival was significantly increased with BBO-8520 treatment to 59 days (p=0.0240) and increased to 48 days with anti-PD-1 treatment, but this increase was not significant (p=0.3952) **(Fig. 6F)**. While there was a statistically significant survival benefit between the anti-PD-1 and combination groups (p=0.0033), there was only a trend towards a survival benefit between the BBO-8520 and combination groups (p=0.1932) because of the strong effect of BBO-8520 monotherapy. All treatments in syngeneic models were well tolerated alone or in combination with anti PD-1 antibody.

BBO-8520 retains activity in models resistant to sotorasib

386 The efficacy of BBO-8520 was next evaluated in the $KRAS^{G12C}$(OFF)-only inhibitor
387 treatment-resistant NSCLC LUN055 PDX model. In addition to bearing a $KRAS^{G12C}$
388 mutation, patient-derived LUN055 cells overexpress the RTK RET. Overexpression of
389 RET is hypothesized to increase the amount of $KRAS^{G12C}$ loaded with GTP, which makes
390 this model more resistant to $KRAS^{G12C}$ (OFF)-only inhibitors [11]. LUN055 tumor-bearing
391 mice treated daily with 30 mg/kg BBO-8520 for 35 days displayed statistically significant
392 and robust anti-tumor activity of 23% mean tumor regression (**Fig. 7A**). Regressions were
393 achieved with free drug concentration of $AUC_{0\text{-}24h}$ of 79 h*ng/mL. The TGI was only 71%
394 following daily oral treatments with 100 mg/kg sotorasib, showing BBO-8520 has
395 significantly greater anti-tumor activity in this model (p=0.0007 for 100 mg/kg sotorasib vs
396 30 mg/kg BBO-8520). In addition, the free drug concentration was 20-fold higher with
397 sotorasib (free $AUC_{0\text{-}24h}$ of 1563 h*ng/mL with 100 mg/kg sotorasib) compared to BBO-
398 8520.

399 Lastly, the anti-tumor efficacy of BBO-8520 in mice bearing sotorasib-resistant
400 CDX tumors was evaluated. MIA PaCa-2 tumors which developed resistance to 10 mg/kg
401 sotorasib starting on day 35 and had tripled their average volume by day 75 of dosing
402 (**Fig. 7B**) were analyzed for $KRAS^{G12C}$ amplification by ddPCR (**Fig. 7C**). Six out of 8
403 sotorasib resistant tumors revealed significant amplification with 6 to 46 copies of
404 $KRAS^{G12C}$ (**Fig. 7C**). The efficacy of BBO-8520 after sotorasib resistance was assessed
405 in a group of 8 mice that were started on 30 mg/kg of BBO-8520 on day 35 post sotorasib.
406 All mice treated daily with 30 mg/kg of BBO-8520 had a statistically significant ($p<0.01$)
407 reduction in tumor volume and deep responses (**Fig. 7D**). Forty percent of these mice
408 (3/8) had complete tumor regressions within 3 weeks of BBO-8520 dosing and had not

re-grown by the end of the study on day 92 (**Fig 7D**). Treatment for >50 days with 30 mg/kg of BBO-8520, even after 35 days of sotorasib was well tolerated **(Supplementary Fig. S5D)**. A similar experiment in the NCI-H358 model confirmed these results (**Supplementary Fig. S6**). The results from this study show that a dual inhibitor like BBO-8520 could achieve efficacy in patients that have progressed on an (OFF)-only inhibitor like sotorasib or adagrasib.

Discussion

The evolution of precision oncology therapeutics starts with suboptimal first-generation molecules and ends with exquisitely potent, best-in-class medicines that provide optimal target coverage and clinical benefit. Second- and third- generation inhibitors also differentiate themselves from predecessors by not only targeting the native oncogene but also inhibiting resistant variants that drive tumor progression. In the $KRAS^{G12C}$ landscape, sotorasib and adagrasib represent first-generation medicines that inhibit $KRAS^{G12C}$ by sequestering the GDP-bound (OFF) form while lacking activity against the GTP-bound (ON) form. The approval of sotorasib and adagrasib has changed clinical practice for patients with $KRAS^{G12C}$ positive NSCLC but their clinical benefit is suboptimal compared to best-in-class driver-oncogene inhibitors in other oncogene-driven NSCLC disease settings. Recent data from a new set of potent $KRAS^{G12C}$ inhibitors like divarasib, D3S-001, and RMC-6291 have provided clinical evidence that better efficacy is possible with better target coverage or by direct inhibition of the (ON) form of $KRAS^{G12C}$. A phase 1 trial including 60 NSCLC patients treated with divarasib reported a confirmed ORR of 53% and PFS of 13 months [20] . This significant gain in

clinical benefit over sotorasib and adagrasib (ORR: ~35% and PFS ~6 mo) by an (OFF)-only inhibitor with no differentiated mechanism of action highlights the suboptimal nature of first-generation $KRAS^{G12C}$ inhibitors. Similarly, clinical data from RMC-6291, a tri-complex inhibitor of $KRAS^{G12C}$ (ON) that requires cyclophilin A, has shown an ORR of 50% in $KRAS^{G12C}$ (OFF) inhibitor-experienced patients, highlighting the importance of inhibiting the (ON) state [13]. Until now, achieving both exquisite potency and coverage of the (OFF) and (ON) form of $KRAS^{G12C}$ with a direct, covalent small molecule targeting the Switch II/helix3 pocket has been deemed technically unattainable. An inhibitor that could accommodate GTP-bound state of $KRAS^{G12C}$, drive exquisite potency, and directly inhibit the (ON) form of $KRAS^{G12C}$ would undoubtedly conform to a novel class of $KRAS^{G12C}$ inhibitors with excellent potential to achieve new levels of clinical benefit in NSCLC patients. In fact, in a recently published study the combination of the (ON) inhibitor RMC-4998 with the (OFF) inhibitor, sotorasib, exerted superior therapeutic efficacy than either alone providing pre-clinical evidence supporting the superiority of the “dual” mechanism hypothesis [21].

We have developed BBO-8520, a direct, covalent small molecule inhibitor that engages $KRAS^{G12C}$ in both the (ON) and (OFF) conformations with sub-nanomolar potency. This dual mode of action enables rapid, true full-target engagement and inhibition of $KRAS^{G12C}$. The unique ability to accommodate GTP-bound conformation results in forcing $KRAS^{G12C}$ (ON) into state 1 which is unable to bind effectors, providing a novel mechanism of action and differentiating from $KRAS^{G12C}$ (OFF)-only inhibitors that are exclusively dependent on GTP-GDP cycling [5, 6, 20]. We show that adding blockade

of effector binding as a mechanism leads to exquisite potency, optimal target coverage and delays the emergence of adaptive resistance often seen with (OFF)-only inhibitors in the clinic.

Increased $KRAS^{G12C}$(ON), through amplification of the mutant allele or by growth factor activated RTKs, appears to be the prominent mechanism of resistance [20, 22-24]. Newly synthesized KRAS most likely is GTP-bound due to a 10-fold higher concentration of GTP than GDP in the cell [25]. Therefore, transcriptional upregulation of the mutant protein provides an easy escape route for cells to overcome (OFF)-only inhibitors. Similarly, RTK activation can effectively overcome (OFF)-only inhibitors by maintaining a high population of $KRAS^{G12C}$(ON) [26]**.** Our observations show that the presence of EGF and HGF have a profound negative effect on the potency of (OFF)-only inhibitors *in vitro*, while amplification of $KRAS^{G12C}$ is also detrimental *in vivo*. In contrast, BBO-8520 maintains exquisite potency in the presence of growth factors, mutant allele amplification and even when mutations are engineered to maintain $KRAS^{G12C}$ in the (ON) form. This superior profile should result in clinical benefits that would hopefully better resemble current best-in-class targeted agents in NSCLC.

BBO-8520 has entered phase 1 clinical trials in patients with $KRAS^{G12C}$ NSCLC that are either naïve or have experienced first-generation (OFF)-only inhibitors (NCT06343402). Our data supports the hypothesis that targeting both the (ON) and (OFF) forms of $KRAS^{G12C}$ results in greater potency, deeper responses, and slowed development of resistance leading to significant benefits over approved, (OFF)-only $KRAS^{G12C}$ inhibitors in NSCLC.

Materials and Methods

Reagents and Cell Cultures

BBO-8520 was synthesized as described in WO 2023/004102, Example 313 (details provided in Supplementary Methods), and stored at room temperature protected from light in a powder form. BBO-8520 was dissolved in 100% DMSO and aliquoted for long-term storage at −20°C.

All cells were purchased from ATCC or JCRB and cultured according to the protocols provided by the supplier. All cell lines were maintained at 37°C in a humidified incubator at 5% CO_2 and were periodically checked for *Mycoplasma*. Cell lines used for *in vivo* studies were confirmed pathogen and *Mycoplasma*-free by IMPACT 1 assessment (IDEXX BioAnalytics) prior to implant. Cell lines were carried for no more than 15 cell passages in this work.

Generation of recombinant proteins: cloning, expression, and purification

All protein reagents were produced in-house by Protein Expression Laboratory, FNLCR. Entry clones containing E. coli optimized DNA sequences (ATUM, Newark, CA) with an upstream tobacco etch virus (TEV) protease cleavage site were used to generate expression clones in pDest-566 (Addgene #11517) using the protocols outlined by Esposito et al., 2009 [27]. *E. coli* BL21 (DE3) STAR (rne131) containing rare tRNAs (pRar) was transformed with the expression plasmids as described [27, 28], and expression and purification were carried out as described [29, 30].

Nucleotide exchange. KRAS proteins were loaded with GppNHp or GTP as described previously [31].

Mass Spectrometry-Based Covalent Engagement Assay

One μM solution of GTP, GppNHp and GDP-loaded KRAS4b$^{G12C/C118S}$ (amino acids 1-169) protein were prepared and dispensed onto plates and then 30 nL of tested compounds from 1 mM DMSO stocks were added to the appropriate wells. At 15 mins, 2 μL of each reaction mixture was pipetted into 15 μL MALDI matrix solution deposited onto plates. The resulting solution was mixed by aspiration, centrifuged at 2,000 *g* for 1 min, and then 1.5 μL aliquots were dispensed on pre-treated MALDI target. MALDI-TOF measurements were performed on Bruker Daltonics rapifleX Tissuetyper TOF-TOF mass spectrometer using linear mode and mass range from 18.6 to 21.6 kDa. Percent modification was calculated as a ratio of peak height for protein modified by compound to sum of peak height of remaining protein plus peak height for protein modified by compound. For the detailed protocol see [32].

Protein-Protein Interaction assay for RAS-RAF disruption

A protein:protein interaction (PPI) Homogeneous Time-Resolved Fluorescence (HTRF) assay was used to determine the effectiveness of compounds in disrupting KRAS protein and effector (RAF1) binding. Avi-KRAS^{G12C} (amino acids 2-169) GTP or GppNHp and RAF1 RBD-3xFLAG (amino acids 51-131) were used. Compounds were dispensed in assay plate (384-well, Grenier Bio-One) using Echo (model 555) with dose response settings: 200 nL final volume, titration from 30 μM as a 10-point dilution series. Proteins

and HTRF reagents were mixed and dispensed onto plates, 20 µL per well, and then incubated for 1 hr at room temperature, with 700 rpm shaking, and data were collected and analyzed as described previously [33].

Crystallization and structure determination

Protein samples for crystallography were prepared by tethering BBO-8520 to KRAS4b(1-169)$^{G12C/C118S}$ bound to GppNHp or GDP. GDP or GppNHp-loaded protein (20.5 mg) was diluted to 100 µM in a buffer containing 20 mM HEPES, 150 mM NaCl, and 2 mM $MgCl_2$ at pH 7.3. A three-fold molar excess of a 10 mM solution of BBO-8520 in DMSO was added, followed by brief mixing at room temperature for 2 mins. Modification completion was confirmed by MALDI-TOF MS. The reaction mixture was purified on a low-pressure chromatographic system (NGC, Bio-Rad) using five in-line connected 5 ml Sephadex G-25 HiTrap desalting columns (Cytiva), the same buffer used for the reaction at 4 mL/min flow rate and monitoring eluent at 280 nm. Protein-containing fractions were collected, and modified protein quality was confirmed by MALDI-TOF MS.

Crystallization screenings were set up using the sitting-drop vapor diffusion method, as described previously [34]. Fifteen mg/mL of the GppNHp-bound tethered KRAS^{G12C} or 40 mg/mL of the GDP-bound tethered KRAS^{G12C} was mixed with an equal volume (200 nL) of the reservoir solution. Crystals of GppNHp-bound KRAS^{G12C} were obtained from a reservoir solution consisting of 56 mM NaH_2PO_4 and 1343 mM K_2HPO_4. Crystals of GDP-bound KRAS^{G12C} were obtained from a reservoir solution consisting of 0.1 M Na_3 citrate pH 5.5, 20% PEG 4000, and 10% isopropanol. Crystals were cryo-protected with 30%

glycerol and flash-frozen in liquid nitrogen. Diffraction data were collected from Argonne National Laboratory (ANL) Advanced Photon Source (APS) beamline 24-ID-C at 100 K and wavelength 0.979 Å. Data were integrated and scaled using XDS [35]. Structure solution was obtained with molecular replacement using Phaser [36] as implemented in the Phenix programs suite, with the MRTX849-bound $KRAS^{G12C}$ (PDB: 6UT0) [37] as the search model. Iterative model building and refinement were performed with COOT and Phenix refine [38]. Crystal parameters, data collection and refinement statistics are summarized in **Supplementary Table S1**. The GppNHp dataset was affected by lattice-translocation disorder in the crystal, but its impact on chain A was minimal. **Supplementary Fig. S2** shows the omit map around BBO-8520, nucleotide, Mg^{2+} ion and C12 in chain A of both structures. Crystallographic and structural analysis software support is provided by the SBGrid consortium [39]. The atomic coordinates and structure factors of the GDP-bound and GppNHp-bound $KRAS^{G12C}$ tethered with BBO-8520 have been deposited in the Protein Data Bank and are available under accession numbers 8VCA and 8VC9, respectively.

^{31}P NMR

All NMR samples included 800 mM of $KRAS^{G12C}$-GTP protein in 93% H_2O/7% D_2O solvent composition in a buffer comprised of 20 mM HEPES (pH 7.3), 150 mM NaCl, 2 mM $MgCl_2$, and 500 µM 2,2-dimethyl-2-silapentanesulfonic acid (DSS) as internal standard, as described previously [14]. Binary and ternary complexes of $KRAS^{G12C}$-GTP-BBO-8520 and $KRAS^{G12C}$-GTP-BBO-8520-RAF1 RBD were prepared in 1:2 and

1:2:1 stoichiometric ratio, respectively. All data were collected on a Bruker 500 MHz spectrometer at 278K. See **Supplementary Materials and Methods** for details.

Western Blotting

Western blot experiments were performed according to the standard protocols. Primary antibodies were obtained from Cell Signaling Technology and were used at a concentration of 1:1000: p-Akt S473 (#9271), AKT (#9272), p-p44/42 MAPK T202/204 (#9101), ERK1/2 (#9102), Vinculin (#13901) and GAPDH (#2118). KRAS4b antibody was purchased from Proteintech (12063-1-AP).

Homogeneous Time-Resolved Fluorescence (HTRF) assay for pERK

Phospho-ERK levels were analyzed as described previously [40].

3D Viability Assay

Cells were seeded at 1,000 cells per well in ultra-low attachment 96-well plates. Two days after plating, cells were treated with a 9-point dose titration of BBO-8520 starting at 10 μM in 1:3 dilution increments using a Tecan D300e. Cells were incubated with BBO-8520 for a period of 4-7 days. After treatment, viability was assessed using a 3D CTG reagent (Promega). Luminescence was read on a Clariostar plate reader, and the data was imported into GraphPad Prism 9, log transformed and normalized to DMSO as 100% and media only as 0%. Following normalization, nonlinear regression was performed on a log (inhibitor) versus normalized response curve fit to generate an IC_{50}.

K_{inact}/K_i measurements

Second-order rate constant K_{inact}/K_i of covalent inhibition of $KRAS^{G12C}$ was determined as described [41] with modifications. Details are provided in **Supplementary Materials and Methods**.

RNA-Seq

Sequence reads were trimmed to remove possible adapter sequences and nucleotides with poor quality using Trimmomatic v.0.36. The trimmed reads were mapped to the Homo sapiens GRCh38 reference genome available on ENSEMBL using the STAR aligner v.2.5.2b to generate BAM files. Unique gene hit counts were calculated using featureCounts from the Subread package v.1.5.2. The hit counts were summarized and reported using the gene_id feature in the annotation file. Only unique reads that fell within exon regions were counted. If a strand-specific library preparation was performed, the reads were strand-specifically counted. After extraction of gene hit counts, the gene hit counts table was used for downstream differential expression analysis. Using DESeq2, a comparison of gene expression between the customer-defined groups of samples was performed. The Wald test was used to generate p-values and log2 fold changes. Genes with an adjusted p-value < 0.05 and absolute log2 fold change > 1 were called as differentially expressed genes for each comparison.

RAS-Raf ELISA assay

MIA Paca-2 cells were seeded at 280,000 cells/well in 1 mL of DMEM with 10% FBS in a 12-well plate and placed in a 37 ◦C incubator and allowed to adhere overnight. Cells were

614 treated with 1 μM of BBO-8520, sotorasib, adagrasib, or GDC-6036 using the Tecan
615 D300e for 2, 5, 10, 15, 30, and 60 mins. Following treatment, the cells were processed
616 according to the manufacturer's protocol (Abcam, Cat# 134640) Luminescence was read
617 on a BMG Labtech Clariostar plate reader and data was exported to GraphPad Prism 9
618 where it was normalized to dimethyl sulfoxide treated cells (DMSO) as 100% and blank
619 as 0%. Following normalization, nonlinear regression was performed on an inhibitor
620 versus normalized response curve fit to generate a time for 50% inhibition for each cell
621 line treated with compound.
622
623 **KRAS$^{G12C/A59G}$ experiments**
624 HeLa cells were engineered to express the KRAS$^{G12C/A59G}$ under the control of the
625 doxycycline-induced promoter. Cells were transduced with lentivirus and selected with 1
626 μg/mL puromycin for several passages. Cells were plated at 1.25e6 cells in 10 cm dish
627 into media containing 200 ng/ml doxycycline, allowed to attach for 24 hrs, then treated for
628 2 hrs with various doses of compound. Following treatment, cell lysates were collected
629 and processed for Western blot using phospho-ERK (Thr202/204), total ERK, KRAS, and
630 vinculin according to the Western blotting methods above.
631
632 ***In vivo* studies**
633 All *in vivo* procedures were reviewed and approved by the Institutional Animal Care and
634 Use Committee prior to execution and performed in accordance with the regulations and

guidelines of the Association for Assessment and Accreditation of Laboratory Animal Care.

In vivo studies were performed at Charles River Accelerator and Development Lab, Crown Biosciences, Inc., GenenDesign Co., Ltd., and NYU Langone Health in accordance with protocols and Institutional Animal Care and Use Committee guidelines. The vehicle used was the BBO-8520 and sotorasib formulation buffer for all studies (10% v/v N-methyl-pyrrolidone (Sigma-Aldrich, catalog 328634), 20% w/v solutol (Sigma-Aldrich, catalog 42966), 30% v/v polyethylene glycol 300 (Sigma-Aldrich, catalog 8074841000) in 50 mM citrate buffer pH 4-5). Plasma compound concentration levels were measured following protein precipitation using LC-MS/MS at Cytoscient, LLC or BioDuro-Sundia, Inc.

For Matrigel plug PK/PD studies, each athymic nude mice was inoculated subcutaneously with $5x10^6$ MIA PaCa-2 tumor cells suspended in growth factor reduced Matrigel (Sigma ECM, Sigma-Aldrich, catalog E6909), and treatments were administered the following day. Plugs were processed into lysates, and pERK tumor levels were measured using MSD (MSD, catalog N45107B-1) according to the manufacturer's instructions. pERK tumor levels normalized to vehicle tumor levels (% pERK (normalized to vehicle) = (experimental (pERK/ERK))/(vehicle (pERK/ERK)) x 100) were reported.

Standard protocols were followed to establish all subcutaneous CDX and PDX models. When CDX or PDX tumors reached a mean size of 175 to 210 mm^3, mice were randomized into treatment groups (n=10 per group) and orally dosed daily for 28 to 35 days. For the sotorasib-resistant efficacy study, MIA PaCa-2 tumor-bearing BALB/c

nude mice were treated orally once daily with vehicle for 54 days or with 10 mg/kg sotorasib until resistance developed on day 35 (tumor volume reached 188 mm^3). These mice were then randomized (10 animals/group) and treated daily with 10 mg/kg sotorasib from day 37 to 85 or with 30 mg/kg BBO-8520 from day 37 to 97. Tumor volumes are shown until one mouse in each group had to be euthanized due to large tumor volume. Standard methods were used to extract genomic DNA from tumors and measure levels of KRAS amplification using pre-designed ddPCR copy number assay probes for human KRAS (Bio-Rad, catalog 10031240) and the reference gene RPP30 (Bio-Rad, catalog 10031241) according to the manufacturer's instructions.

For the NSCLC GEMM efficacy study, $KRAS^{G12C}$;$Tp53^{R270H}$ mice (mixed background;[18]) were monitored by MRI for tumor development after intranasal induction with adeno-Cre (2.5×10^6 PFU). When lung tumors reached a mean size of 84 mm^3, mice were randomized into treatment groups (n=10 per group) and orally dosed daily with vehicle or 10 mg/kg BBO-8520 for 42 days. Lung tumor volume was monitored by MRI every 2 weeks.

For the syngeneic liver tumor model efficacy study, the murine CRC $KRAS^{G12D}$ CT26-g-GFP/luciferase cell line (Creative Biogene, catalog CSC-RR0238) was engineered to introduce the $KRAS^{G12C}$ mutation. Each anesthetized BALB/c mouse was injected into the liver with 5 x 10^5 CT26-$KRAS^{G12C}$-luciferase tumor cells suspended in PBS. Standard methods were used to measure bioluminescence signal with an IVIS Spectrum (Perkin Elmer). When liver tumor bioluminescence signal reached a mean of $3.6x10^6$ photons/second, mice were randomized into treatment groups (n=10 per group) and

dosed orally with vehicle or BBO-8520 until day 28 or intraperitoneally anti-PD-1 (clone RMP1-14, Bio X Cell, catalog BE0146) biweekly for 3 weeks. Mice were euthanized when bioluminescence signal was > 8.9 x 10^8 photons/ seconds or when they showed defined signs of a large tumor.

Data analyses were performed using Microsoft Excel or GraphPad Prism software (version 9). For statistical analyses comparing pERK Matrigel plug levels in the vehicle group to all other groups, one-way ANOVA of all group means followed by post hoc Dunnett's multiple comparisons were performed using GraphPad Prism software. For the statistical analyses comparing the vehicle group to all other groups in the efficacy studies, two-way repeated measures or mixed-effects ANOVA followed by post hoc Dunnett's multiple comparisons test of the means was applied over the indicated number of days using GraphPad Prism software.

Data Availability

The data generated in these analyses are available within the article and its supplementary data files. The RNA-Seq data generated in this study are publicly available in Gene Expression Omnibus (GEO) at (GSE278656). The atomic coordinates and structure factors of the GDP-bound and GppNHp-bound KRAS-G12C tethered with BBO-8520 have been deposited in the Protein Data Bank and are available under accession numbers 8VCA and 8VC9, respectively.

ACKNOWLEDGMENTS

We thank William Burgan, Katie Powell, Scott Eury, Lauryl Scott, Nick Wright, Vanessa Wall, Bill Gillette, Simon Messing, Mukul Sherekar, Jennifer Mehalko, Shelley Perkins, Peter Frank, Troy Taylor, Nitya Ramakrishnan, and Brianna Higgins of the Protein Expression Laboratory (Frederick National Laboratory for Cancer Research) for their help in generating cell lines and recombinant proteins. We thank Monalisa Swain for her help with SPR experiments. We thank Mariam Ashraf, Derek Bratcher, and Sathiya Dharmaiah for their help in protein crystallization. We thank Kyle Sullivan, Nadage Gitego, Cindy Feng and Carlos Stahlhut for non-$KRAS^{G12C}$ cell line IC_{50} measures. X-ray diffraction data were collected at Northeastern Collaborative Access Team beamlines (24-ID-C), funded by the NIH (NIGMS P30 GM124165). The Pilatus 6M detector on the 24-ID-C beamline is supported by an NIH-ORIP HEI grant (S10 RR029205). This research utilized resources at the Advanced Photon Source, operated by Argonne National Laboratory for the US Department of Energy Office of Science (Contract DE-AC02-06CH11357). Part of this work was supported by Lawrence Livermore National Laboratory under Contract No. DE-AC52-07NA27344 (Release: LLNL-JRNL-864652). We thank the computing support from Lawrence Livermore National Laboratory institutional grand challenge program. This project has been funded in part with Federal funds from the National Cancer Institute, National Institutes of Health, under Contract No. 75N91019D00024. The content of this publication does not necessarily reflect the views or policies of the Department of Health and Human Services nor does mention of trade names, commercial products, or organizations imply endorsement by the US government.

References

1. Zehir, A., R. Benayed, R.H. Shah, A. Syed, S. Middha, H.R. Kim, et al., *Mutational landscape of metastatic cancer revealed from prospective clinical sequencing of 10,000 patients.* Nat Med, 2017. **23**(6): p. 703-713.
2. Moore, A.R., S.C. Rosenberg, F. McCormick, and S. Malek, *RAS-targeted therapies: is the undruggable drugged?* Nat Rev Drug Discov, 2020. **19**(8): p. 533-552.
3. Nassar, A.H., E. Adib, and D.J. Kwiatkowski, *Distribution of KRAS (G12C) Somatic Mutations across Race, Sex, and Cancer Type.* N Engl J Med, 2021. **384**(2): p. 185-187.
4. Lito, P., M. Solomon, L.S. Li, R. Hansen, and N. Rosen, *Allele-specific inhibitors inactivate mutant KRAS G12C by a trapping mechanism.* Science, 2016. **351**(6273): p. 604-8.
5. Canon, J., K. Rex, A.Y. Saiki, C. Mohr, K. Cooke, D. Bagal, et al., *The clinical KRAS(G12C) inhibitor AMG 510 drives anti-tumour immunity.* Nature, 2019. **575**(7781): p. 217-223.
6. Hallin, J., L.D. Engstrom, L. Hargis, A. Calinisan, R. Aranda, D.M. Briere, et al., *The KRAS(G12C) Inhibitor MRTX849 Provides Insight toward Therapeutic Susceptibility of KRAS-Mutant Cancers in Mouse Models and Patients.* Cancer Discov, 2020. **10**(1): p. 54-71.

7. Soria, J.C., Y. Ohe, J. Vansteenkiste, T. Reungwetwattana, B. Chewaskulyong, K.H. Lee, et al., *Osimertinib in Untreated EGFR-Mutated Advanced Non-Small-Cell Lung Cancer.* N Engl J Med, 2018. **378**(2): p. 113-125.
8. Peters, S., D.R. Camidge, A.T. Shaw, S. Gadgeel, J.S. Ahn, D.W. Kim, et al., *Alectinib versus Crizotinib in Untreated ALK-Positive Non-Small-Cell Lung Cancer.* N Engl J Med, 2017. **377**(9): p. 829-838.
9. Awad, M.M., S. Liu, Rybkin, II, K.C. Arbour, J. Dilly, V.W. Zhu, et al., *Acquired Resistance to KRAS(G12C) Inhibition in Cancer.* N Engl J Med, 2021. **384**(25): p. 2382-2393.
10. Tanaka, N., J.J. Lin, C. Li, M.B. Ryan, J. Zhang, L.A. Kiedrowski, et al., *Clinical Acquired Resistance to KRAS(G12C) Inhibition through a Novel KRAS Switch-II Pocket Mutation and Polyclonal Alterations Converging on RAS-MAPK Reactivation.* Cancer Discov, 2021. **11**(8): p. 1913-1922.
11. Lietman, C.D., M.L. Johnson, F. McCormick, and C.R. Lindsay, *More to the RAS Story: KRAS(G12C) Inhibition, Resistance Mechanisms, and Moving Beyond KRAS(G12C).* Am Soc Clin Oncol Educ Book, 2022. **42**: p. 1-13.
12. Schulze, C.J., K.J. Seamon, Y. Zhao, Y.C. Yang, J. Cregg, D. Kim, et al., *Chemical remodeling of a cellular chaperone to target the active state of mutant KRAS.* Science, 2023. **381**(6659): p. 794-799.
13. Jänne, P.A., F. Bigot, K. Papadopoulos, L. Eberst, D. Sommerhalder, L. Lebellec, et al., *Abstract PR014: Preliminary safety and anti-tumor activity of RMC-6291, a first-in-class, tri-complex KRASG12C(ON) inhibitor, in patients with or without*

prior KRASG12C(OFF) inhibitor treatment. Molecular Cancer Therapeutics, 2023. **22**(12_Supplement): p. PR014-PR014.

14. Sharma, A.K., J. Pei, Y. Yang, M. Dyba, B. Smith, D. Rabara, et al., *Revealing the mechanism of action of a first-in-class covalent inhibitor of KRASG12C (ON) and other functional properties of oncogenic KRAS by (31)P NMR.* J Biol Chem, 2024: p. 105650.
15. Spoerner, M., C. Hozsa, J.A. Poetzl, K. Reiss, P. Ganser, M. Geyer, et al., *Conformational states of human rat sarcoma (Ras) protein complexed with its natural ligand GTP and their role for effector interaction and GTP hydrolysis.* J Biol Chem, 2010. **285**(51): p. 39768-78.
16. Esposito, D., A.G. Stephen, T.J. Turbyville, and M. Holderfield, *New weapons to penetrate the armor: Novel reagents and assays developed at the NCI RAS Initiative to enable discovery of RAS therapeutics.* Semin Cancer Biol, 2019. **54**: p. 174-182.
17. Patricelli, M.P., M.R. Janes, L.S. Li, R. Hansen, U. Peters, L.V. Kessler, et al., *Selective Inhibition of Oncogenic KRAS Output with Small Molecules Targeting the Inactive State.* Cancer Discov, 2016. **6**(3): p. 316-29.
18. Li, S., S. Liu, J. Deng, E.A. Akbay, J. Hai, C. Ambrogio, et al., *Assessing Therapeutic Efficacy of MEK Inhibition in a KRAS(G12C)-Driven Mouse Model of Lung Cancer.* Clin Cancer Res, 2018. **24**(19): p. 4854-4864.
19. Fedele, C., S. Li, K.W. Teng, C.J.R. Foster, D. Peng, H. Ran, et al., *SHP2 inhibition diminishes KRASG12C cycling and promotes tumor microenvironment remodeling.* J Exp Med, 2021. **218**(1).

20. Sacher, A., P. LoRusso, M.R. Patel, W.H. Miller, Jr., E. Garralda, M.D. Forster, et al., *Single-Agent Divarasib (GDC-6036) in Solid Tumors with a KRAS G12C Mutation.* N Engl J Med, 2023. **389**(8): p. 710-721.
21. Nokin, M.J., A. Mira, E. Patrucco, B. Ricciuti, S. Cousin, I. Soubeyran, et al., *RAS-ON inhibition overcomes clinical resistance to KRAS G12C-OFF covalent blockade.* Nat Commun, 2024. **15**(1): p. 7554.
22. Ryan, M.B., O. Coker, A. Sorokin, K. Fella, H. Barnes, E. Wong, et al., *KRAS(G12C)-independent feedback activation of wild-type RAS constrains KRAS(G12C) inhibitor efficacy.* Cell Rep, 2022. **39**(12): p. 110993.
23. Ryan, M.B., F. Fece de la Cruz, S. Phat, D.T. Myers, E. Wong, H.A. Shahzade, et al., *Vertical Pathway Inhibition Overcomes Adaptive Feedback Resistance to KRAS(G12C) Inhibition.* Clin Cancer Res, 2020. **26**(7): p. 1633-1643.
24. Xue, J.Y., Y. Zhao, J. Aronowitz, T.T. Mai, A. Vides, B. Qeriqi, et al., *Rapid non-uniform adaptation to conformation-specific KRAS(G12C) inhibition.* Nature, 2020. **577**(7790): p. 421-425.
25. Huang, L., Z. Guo, F. Wang, and L. Fu, *KRAS mutation: from undruggable to druggable in cancer.* Signal Transduct Target Ther, 2021. **6**(1): p. 386.
26. Akhave, N.S., A.B. Biter, and D.S. Hong, *Mechanisms of Resistance to KRAS(G12C)-Targeted Therapy.* Cancer Discov, 2021. **11**(6): p. 1345-1352.
27. Esposito, D., L.A. Garvey, and C.S. Chakiath, *Gateway cloning for protein expression.* Methods Mol Biol, 2009. **498**: p. 31-54.

28. Wall, V.E., L.A. Garvey, J.L. Mehalko, L.V. Procter, and D. Esposito, *Combinatorial assembly of clone libraries using site-specific recombination.* Methods Mol Biol, 2014. **1116**: p. 193-208.
29. Taylor, T. and W. Gillette, *Production of Isotopically Labeled KRAS4b.* Methods Mol Biol, 2024. **2797**: p. 23-34.
30. Kopra, K., E. Vuorinen, M. Abreu-Blanco, Q. Wang, V. Eskonen, W. Gillette, et al., *Homogeneous Dual-Parametric-Coupled Assay for Simultaneous Nucleotide Exchange and KRAS/RAF-RBD Interaction Monitoring.* Anal Chem, 2020. **92**(7): p. 4971-4979.
31. Waybright, T. and A.G. Stephen, *Nucleotide Exchange on RAS Proteins Using Hydrolysable and Non-hydrolysable Nucleotides.* Methods Mol Biol, 2024. **2797**: p. 35-46.
32. Dyba, M., J.P. Denson, and A.E. Maciag, *MALDI-TOF Mass Spectrometry-Based Assay for Measuring Covalent Target Engagement of KRAS G12C Inhibitors.* Methods Mol Biol, 2024. **2797**: p. 145-157.
33. Larsen, E.K., M. Abreu-Blanco, D. Rabara, and A.G. Stephen, *KRAS4b:RAF-1 Homogenous Time-Resolved Fluorescence Resonance Energy Transfer Assay for Drug Discovery.* Methods Mol Biol, 2024. **2797**: p. 159-175.
34. Chan, A.H. and D.K. Simanshu, *Crystallographic Studies of KRAS in Complex with Small Molecules and RAS-Binding Proteins.* Methods Mol Biol, 2024. **2797**: p. 47-65.
35. Kabsch, W., *Xds.* Acta Crystallogr D Biol Crystallogr, 2010. **66**(Pt 2): p. 125-32.

36. McCoy, A.J., R.W. Grosse-Kunstleve, P.D. Adams, M.D. Winn, L.C. Storoni, and R.J. Read, *Phaser crystallographic software.* J Appl Crystallogr, 2007. **40**(Pt 4): p. 658-674.
37. Fell, J.B., J.P. Fischer, B.R. Baer, J.F. Blake, K. Bouhana, D.M. Briere, et al., *Identification of the Clinical Development Candidate MRTX849, a Covalent KRAS(G12C) Inhibitor for the Treatment of Cancer.* J Med Chem, 2020. **63**(13): p. 6679-6693.
38. Adams, P.D., P.V. Afonine, G. Bunkoczi, V.B. Chen, I.W. Davis, N. Echols, et al., *PHENIX: a comprehensive Python-based system for macromolecular structure solution.* Acta Crystallogr D Biol Crystallogr, 2010. **66**(Pt 2): p. 213-21.
39. Morin, A., B. Eisenbraun, J. Key, P.C. Sanschagrin, M.A. Timony, M. Ottaviano, et al., *Collaboration gets the most out of software.* Elife, 2013. **2**: p. e01456.
40. Smith, B.P., M. Rigby, R. Ma, and A.E. Maciag, *High-Throughput Cell-Based Screening of Small Molecule KRAS Signaling Inhibitors Using a Homogeneous Time-Resolved Fluorescence (HTRF) Assay.* Methods Mol Biol, 2024. **2797**: p. 271-285.
41. Li, K.S., J.G. Quinn, M.J. Saabye, J.F.S. Guerrero, J. Nonomiya, Q. Lian, et al., *High-Throughput Kinetic Characterization of Irreversible Covalent Inhibitors of KRAS(G12C) by Intact Protein MS and Targeted MRM.* Anal Chem, 2022. **94**(2): p. 1230-1239.

Figure Legends

Figure 1. Discovery of BBO-8520. **A**, The compound progression chart shows the development of BBO-8520. Non-covalent KRAS^{G12D} inhibitor, Compound **1,** showed binding activity (SPR) to GppNHp-bound KRAS^{G12D}, and disruption of KRAS^{G12D}/RAF1(RBD) interaction in PPI assay. Compound **1** was equipped with a covalent warhead to generate Compound **2**. Optimization of cell potency and ADME properties gave rise to Compound **3**. Further improvement of the GTP-bound KRAS^{G12C} activity by replacing the aminobenzothiazole of Compound **3** with a cyano-amino benzothiophene at quinazoline 7-position gave rise to BBO-8520. BBO-8520 shows covalent labelling of C12 in the active, GppNHp- or GTP-bound KRAS^{G12C}, as well as disruption of KRAS^{G12C}/RAF1(RBD) binding. **B**, The table summarizes the ability of compounds to modify C12 of GDP-, GppNHp-, and GTP-bound KRAS^{G12C} as measured by MALDI-TOF mass spectrometry; and their ability to disrupt GppNHp- or GTP-bound KRAS^{G12C} binding to RAF1(RBD) in PPI assay. **C**, K_{Inact}/K_I measurements of sotorasib, adagrasib, and BBO-8520 in the GDP-bound (OFF) and GTP-bound (ON) conformations of KRAS^{G12C}.

Figure 2. Binding Mode of BBO-8520 to KRAS^{G12C} (ON) and (OFF) conformation. **A**, GDP-bound (OFF) (top, PDB 8V3A) and GppNHp-bound (ON) (bottom, PDB 8V39) forms in surface and ribbon representations. The protein is colored light orange (OFF) or light blue (ON), with Switch-I, Switch-II, and Helix 3 highlighted in pink, cyan, and orange, respectively. BBO-8520 (light green in top panel, pink in bottom panel), nucleotide, C12

878 and T35 are shown as sticks, and Mg2+ (green) and the coordinating waters (red) are
879 shown as spheres. **B, C,** Enlarged view of the binding pocket in the GDP-bound form
880 (PDB 8V3A), focusing on the regions around **(B)** Switch-II and Helix 3, and **(C)** C12 and
881 GDP. The protein and BBO-8520 are colored light orange and light green, respectively.
882 H-bonds are indicated by dashed lines. **D, E,** Enlarged view of the binding pocket in the
883 GppNHp-bound form (PDB 8V39), focusing on the regions around **(D)** Switch-II and Helix
884 3, and **(E)** C12 and GppNHp. The protein and BBO-8520 are colored light blue and light
885 pink, respectively. **F, G,** Overlay of the GDP-bound and GppNHp-bound structures,
886 focusing on the regions around **(F)** Switch-II and Helix 3, and **(G)** C12 and the nucleotide.
887
888 **Figure 3. Mechanism of action and selectivity of BBO-8520. A**, BBO-8520 (ligand (L))
889 binding to $KRAS^{G12C}$-GTP (protein (P)) shifts the state 1 - state 2 equilibrium of protein to
890 the inactive, state 1- like conformation (induced γ_{1PL} peak located most downfield) in the
891 protein-ligand (PL) binary complex spectrum. Peak β_{1PL} represents L binding induced
892 inactive conformation of β GTP. Chemical shifts corresponding to peaks α_1, β_1, and γ_1
893 belong to state 1 (inactive, effector binding- deficient) conformation, whereas α_2, β_2, and
894 γ_2 to the state 2 (active, effector binding-enabled) conformation. RAF1 RBD loading is
895 unable to induce γ_2 (active conformation) population (see P+L+RBD spectrum). Shown
896 on top and bottom are the control spectra (in the presence of DMSO) of P+RBD and P,
897 respectively. The γ_{1PL} peak emergence is only noted in the presence of inhibitor. The
898 control spectra of $KRAS^{G12C}$-GTP alone or in the presence of RBD do not show this peak.
899 **B**, BBO-8520 inhibits SOS-mediated nucleotide exchange of GDP with BODIPY-GDP
900 KRAS. Avi-KRAS mutants indicated and Avi-NRAS WT were loaded with BODIPY-GDP,

then BBO-8520 was added in a 2-fold dilution series starting at 30 nM. The assay was started by the addition of SOS1 (aa564-1048) and GDP, then analyzed after 4 and 24 hrs incubation. $KRAS^{G12C}$ shows the highest inhibition of nucleotide exchange with BBO-8520. NRAS WT was used as a control. **C**, pERK inhibitory activity of BBO-8520, sotorasib and adagrasib against a panel of mouse embryonic fibroblasts (MEFs) driven by KRAS mutants, HRAS, NRAS and $BRAF^{V600E}$. BBO-8520 demonstrates best pERK inhibitory activity in $KRAS^{G12C}$-driven MEF cells, compared to MEFs driven by other KRAS mutants or WT KRAS. BBO-8520 shows no pERK inhibitory activity in MEFs driven by HRAS, NRAS or $BRAF^{V600E}$.

Figure 4. BBO-8520 Potently Inhibits $KRAS^{G12C}$ Signaling in Tumor Cells. A, Target engagement and ERK phosphorylation time course in the $KRAS^{G12C}$ cancer cell lines MIA PaCa-2 and SW1473. BBO-8520 at 20 nM displays rapid pERK inhibition at 30 min which is sustained for up to 24 hrs and is compared to 20 or 100 nM sotorasib and adagrasib, which take longer and show less inhibition of pERK. **B**, HTRF analysis of phosphorylated ERK demonstrates time and dose dependent inhibition in response to BBO-8520 in MIA PaCa-2 and SW1463 cells which is sustained for up 34 hrs post-treatment. **C, D, E**, Potent effects of BBO-8520 on 2 hrs pERK inhibition, pAKT inhibition, and 7-day 3D viability measurements in $KRAS^{G12C}$ cell lines as compared to sotorasib, adagrasib and RMC-6291. The activity of BBO-8520 in $KRAS^{G12C}$ cell lines is compared against a cell line panel comprised of KRAS wild type along with G12C/D/V and S, G13D, and $BRAF^{V600E}$mutants. IC_{50} (nM) values for each cell line are captured on Supplementary Table 2.

Figure 5: BBO-8520 Maintains Potency in Active State of KRAS^{G12C}. A, RAS:RAF ELISA assay in MIA PaCa-2 cells shows rapid dissociation of KRAS^{G12C} (ON) with RAF1 by BBO-8520 compared to the (OFF)-only KRAS^{G12C} inhibitors sotorasib, adagrasib or GDC-6036. **B, C**, NCI-H358 cells were serum starved and then treated with 100 ng/ml of EGF, compound, and assayed for pERK HTRF 20 minutes after compound addition **(B)** or treated with 100 ng/ml of HGF and compound and assayed for a 5-day viability assay **(C)**. Average potency shifts are shown to the right demonstrating the fold changes of IC_{50} following EGF or HGF stimulation compared to vehicle. **D**, HeLa cells were engineered to express a KRAS$^{G12C/A59G}$ double mutant known for attenuated GTP hydrolysis, and assayed for pERK inhibition following treatment with 0.3, 1, 3, and 10 μM of BBO-8520, sotorasib, or adagrasib. BBO-8520 demonstrated a potent inhibition of the pERK signal compared to the (OFF)-only inhibitors, which showed no activity. **E**, A long-term clonogenic assay using IC_{90} concentrations (2-hr pERK) of BBO- 8520, sotorasib and adagrasib, shows that only BBO-8520 can drive complete growth suppression for up to 35 days in culture compared to sotorasib or adagrasib.

Figure 6. BBO-8520 Demonstrates Dose- and Time-Dependent Inhibition of pERK and Strong Efficacy in KRAS^{G12C} Models. A, BBO-8520 shows dose-responsive inhibition of pERK at 6 hrs following a dose of 3, 10, and 30 mg/kg in a MIA PaCa-2 Matrigel plug PD assay (*p<0.01, **p<0.0001). **B**, Suppression of pERK was observed up to 72 hrs following treatment with 30 mg/kg of BBO-8520 in the MIA PaCa-2 Matrigel plug PD (*p<0.01, **p<0.0001). **C**, In the corresponding MIA PaCa-2 CDX model, BBO-8520

showed significant anti-tumor activity at 0.1, 0.3, 1, 3, and 10 mg/kg following 28 days of treatment (*p<0.0001). **D**, In the NCI-H358 CDX model, BBO-8520 demonstrated significant and robust efficacy at 0.3, 1, 3, and 10 mg/kg following 28 days of treatment (*p<0.0001). **E**, In the KCP NSCLC GEMM, BBO- 8520 demonstrated significant and robust efficacy at 10 mg/kg (*p<0.0001). **F**, In the CT26-KRAS^{G12C}- luciferase syngeneic liver tumor model, BBO-8520 extended the median survival as a monotherapy or in combination with anti-PD-1.

Figure 7. BBO-8520 is More Efficacious Than Sotorasib and Shows Activity in Sotorasib-Resistant Tumors. A, Efficacy of BBO-8520 and sotorasib in the RET amplified LUN055 PDX model. Both BBO-8520 and sotorasib demonstrate anti-tumor activity (*p<0.0001), with BBO-8520 showing significant tumor regressions (23%) vs. 71% TGI for sotorasib. **B**, MIA PaCa-2 xenografts were grown under the presence of 10 mg/kg of sotorasib until tumors became resistant under treatment (day35). On day 35, a cohort of 8 mice were switched from sotorasib (10 mg/kg) to 30 mg/kg of BBO-8520. These mice showed strong responses with tumor volume regression. **C,** Analysis of sotorasib resistant tumors show a high proportion of KRAS^{G12C} amplification by ddPCR. **D,** Focused view of mice continuing on 10 mg/kg sotorasib or switched to 30 mg/kg BBO-8520 starting on day 35 (200 mm^3)**.** All mice treated with BBO-8520 had a statistically significant (p<0.01) reduction in tumor volume compared to those continued on sotorasib. This included three mice with complete tumor regressions.

Figure 1

A

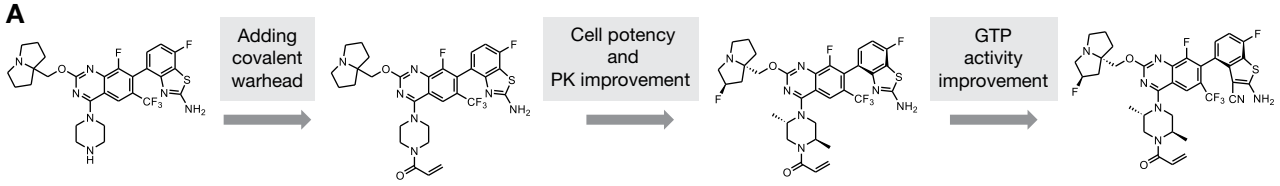

Compound 1
SPR: $KRAS^{G12D}$ GppNHpKD (μM): 0.52
PPI: $KRAS^{G12D}$/RAF1 (μM): 1.4

Compound 2 | **Compound 3** | **BBO-8520**

B

Compounds	MALDI-TOF MS % modification, 15 min			PPI: $KRAS^{G12C}$/RAF1 (μM)	
	GDP	GppNHp	GTP	GppNHp	GTP
Compound 2	80	50	NA	0.14	NA
Compound 3	93	97	38	0.12	3.19
BBO-8520	100	100	89	0.026	0.10
sotorasib	88	0	3	>30	>30
adagrasib	82	0	1	>30	>30

C

		Kinact/KI ($M^{-1}s^{-1}$)	
		GDP	GTP
Mass Spec	sotorasib	11,000	0
	adagrasib	180,000	0
	BBO-8520	2,743,000	20,000

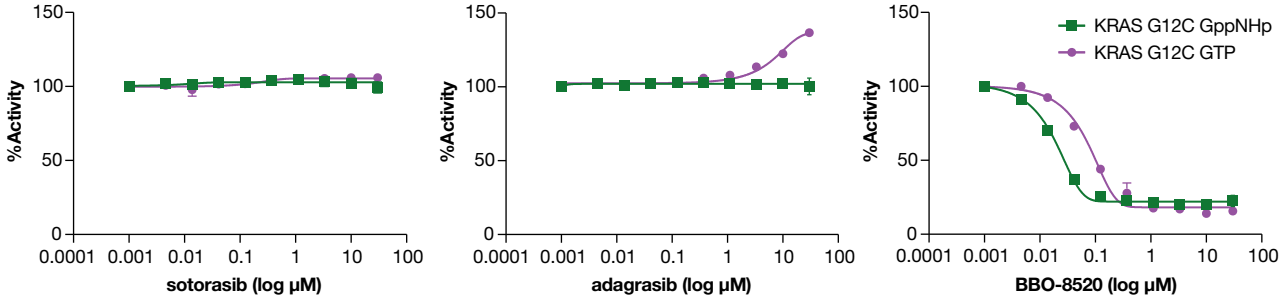

Figure 2

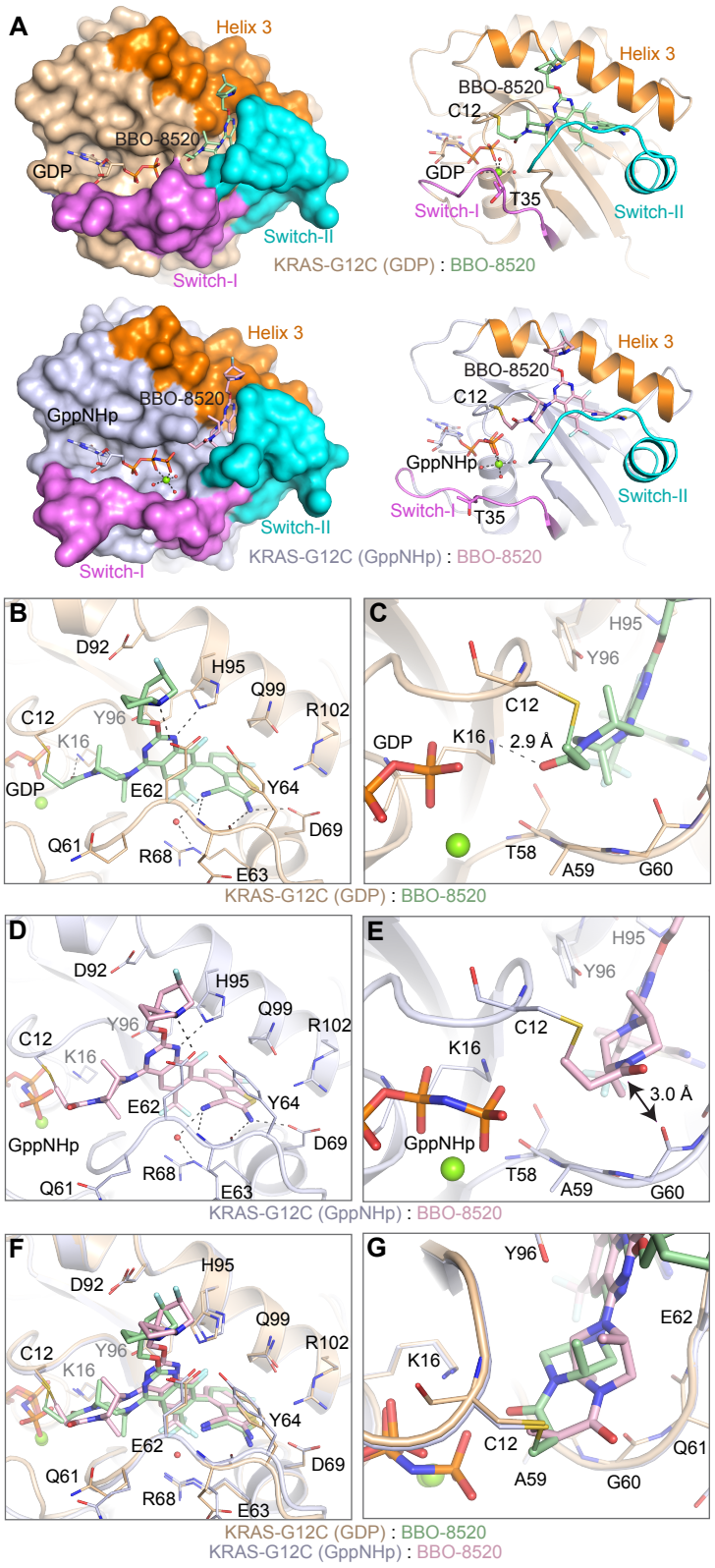

Figure 3

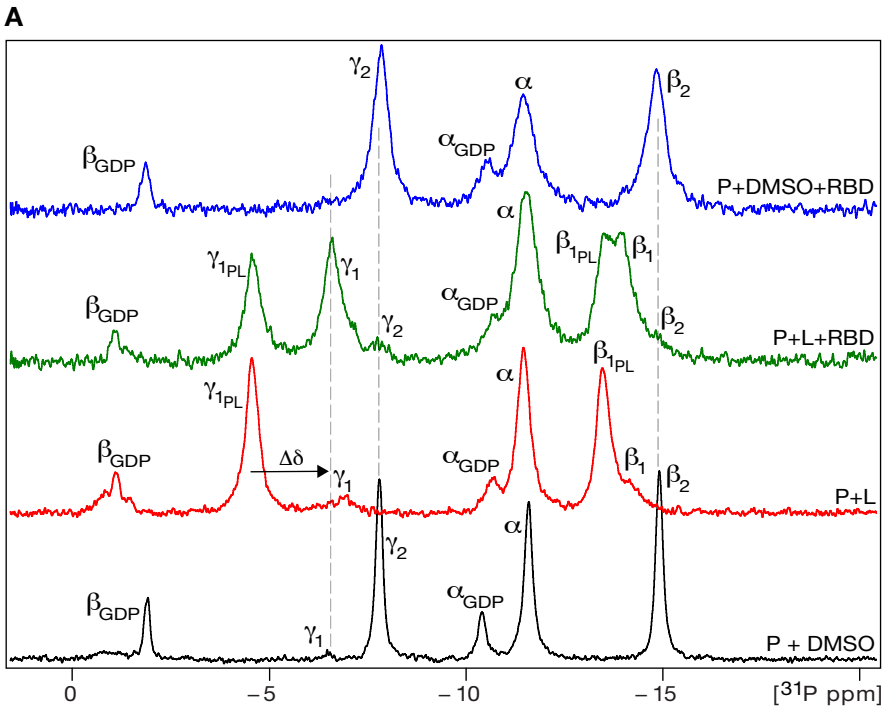

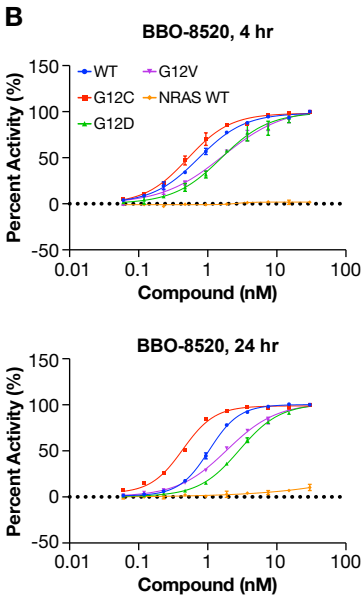

C

	BBO-8520 pERK IC_{50} (nM)		sotorasib pERK IC_{50} (nM)		adagrasib pERK IC_{50} (nM)	
MEF Cell Line	**2 hr**	**4 hr**	**2 hr**	**4 hr**	**2 hr**	**4 hr**
KRAS G12C	10	2.7	145	45	355	98
KRAS G12D	447	410	>10,000	>10,000	>10,000	>10,000
KRAS G12V	4,700	4,130	>10,000	>10,000	>10,000	>10,000
KRAS G13D	31	30	>10,000	>10,000	>10,000	>10,000
KRAS Q61R	>10,000	>10,000	>10,000	>10,000	>10,000	>10,000
KRAS4b WT	29	13	>10,000	>10,000	>10,000	>10,000
KRAS4a WT	283	287	>10,000	>10,000	>10,000	>10,000
HRAS WT	8,260	>10,000	>10,000	>10,000	>10,000	>10,000
NRAS WT	>10,000	>10,000	>10,000	>10,000	>10,000	>10,000
BRAF V600E	>10,000	>10,000	>10,000	>10,000	>10,000	>10,000

Figure 4

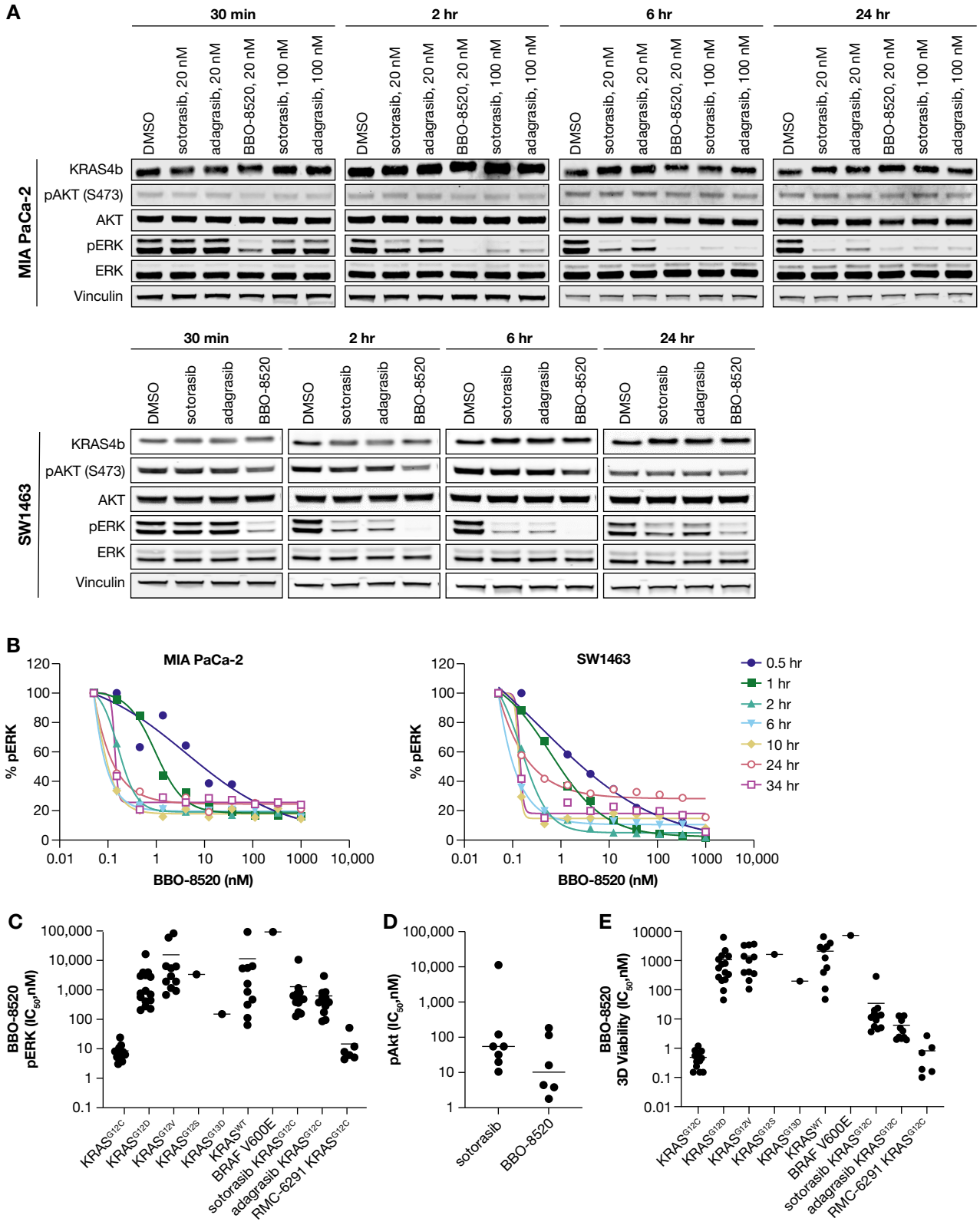

Figure 5

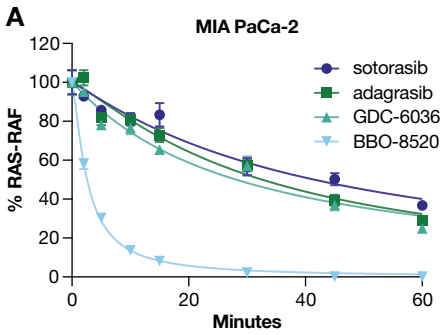

Compound	Time to 50% Inhibition (Minutes)	% sotorasib, Time to 50% Inhibition,
sotorasib	41.5	100.0
adagrasib	32.6	78.5
GDC-6036	28.2	67.8
BBO-8520	2.6	6.3

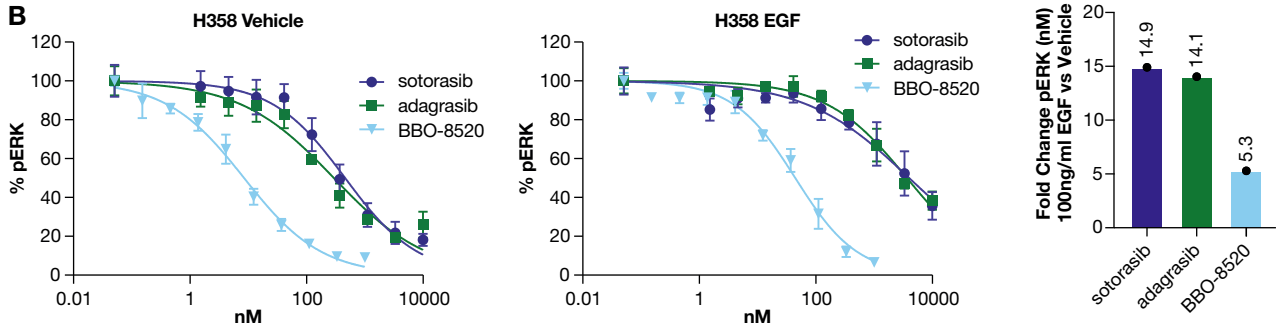

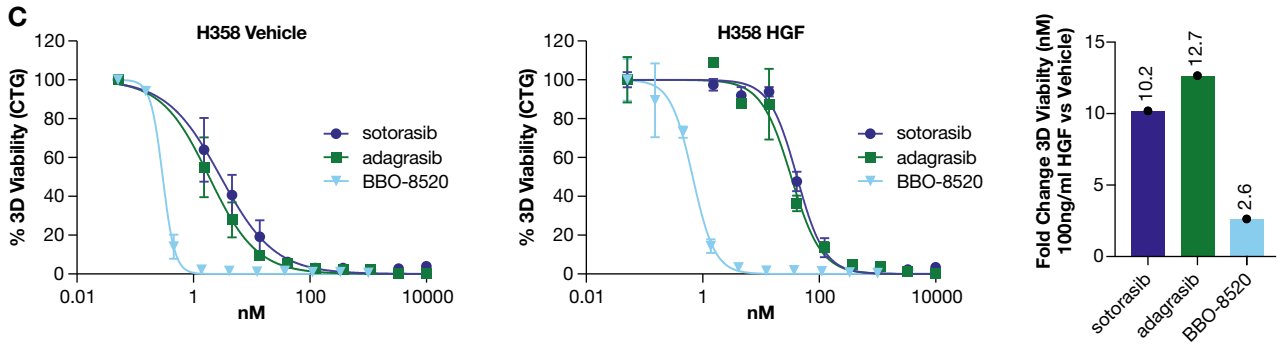

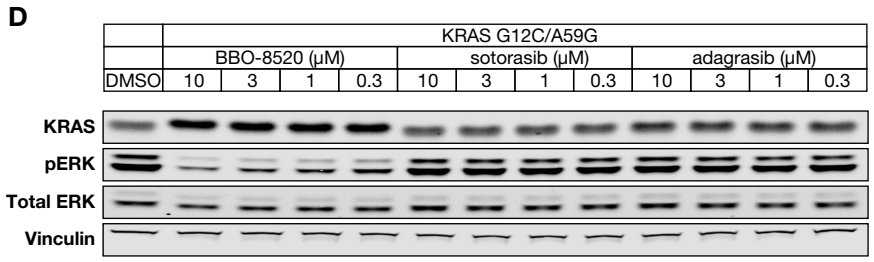

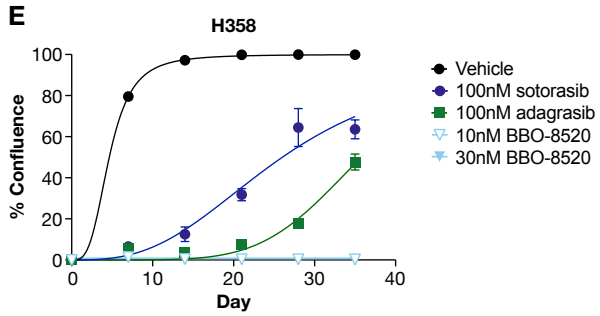

Figure 6

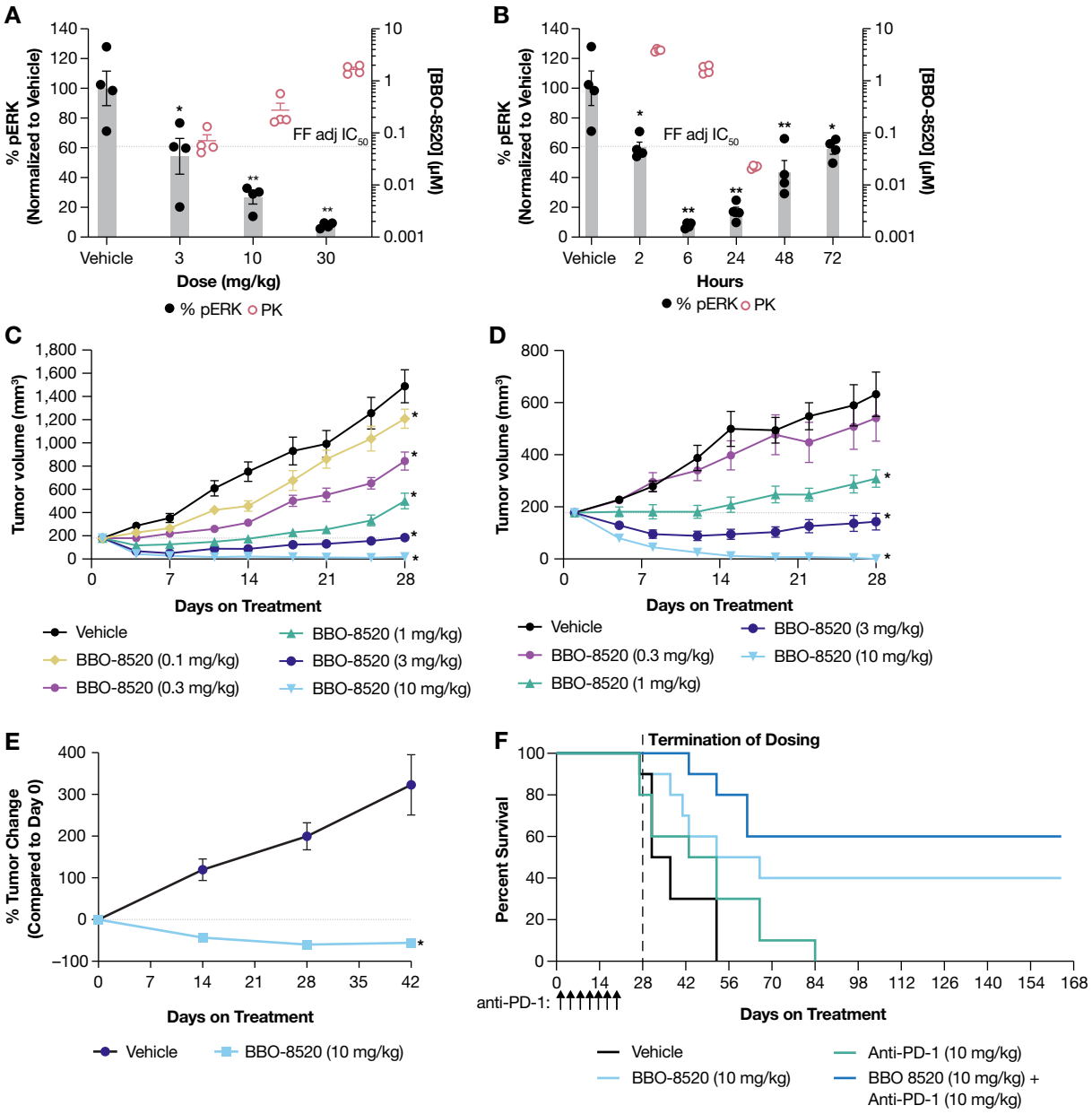

Figure 7